Electronic Supplementary Material (ESI) for Inorganic Chemistry Frontiers.

Electronic Supplementary Information

Superstable 3p-block metal-organic framework platform towards prominent CO_2 and C1/C2-hydrocarbon uptake and separation performance and strong Lewis acid catalysis for CO_2 fixation

Jian-Wei Zhang,[a,b†] Wen-Juan Ji,[a,c†] Man-Cheng Hu,[a] Shu-Ni Li,[a] Yu-Cheng Jiang,[a] Xian-Ming Zhang*[c], Peng Qu[b] and Quan-Guo Zhai*[a]

[a] Key Laboratory of Macromolecular Science of Shaanxi Province, Key Laboratory of Applied Surface and Colloid Chemistry, Ministry of Education, School of Chemistry & Chemical Engineering, Shaanxi Normal University, Xi'an, Shaanxi, 710062, China
E-mail: zhaiqg@snnu.edu.cn

[b] Henan Key Laboratory of Biomolecular Recognition and Sensing, School of Chemistry and Chemical Engineering, Shangqiu Normal University, Shangqiu, 476000, China

[c] Key Laboratory of Magnetic Molecules & Magnetic Information Materials, Ministry of Education, School of Chemistry & Materials Science, Shanxi Normal University, Linfen, Shanxi, 041004, China. E-mail: zhangxm@dns.sxnu.edu.cn

† These authors contributed equally to this work.

Table S1. Crystal data and structure refinements of SNNU-5-Al/Ga/In.

Compound	**SNNU-5-Al**	**SNNU-5-Ga**	**SNNU-5-In**
Empirical formula	$C_{42}H_{22}Al_3O_{16}$	$C_{42}H_{22}Ga_3O_{16}$	$C_{42}H_{22}In_3O_{16}$
Formula weight	863.54	991.76	1127.06
Temperature (K)	100(2)	153(2)	293(2)
Crystal system	Trigonal	Trigonal	Trigonal
Space group	*R*-3*c*	*R*-3*c*	*R*-3*c*
a(Å)	27.3814(9)	27.3458(4)	28.1880(6)
b(Å)	27.3814(9)	27.3458(4)	28.1880(6)
c(Å)	71.344(5)	72.965(2)	74.414(2)
α (deg)	90	90	90
β (deg)	90	90	90
γ (deg)	120	120	120
Volume(Å^3)	46324(4)	47252.7(17)	51205(2)
Z	18	18	18
*d*calcd. (g·cm^{-3})	0.557	0.627	0.658
μ(mm^{-1})	0.066	0.793	0.629
F(000)	7938	8910	9882
Reflections collected/unique	376501/10617	436274/10826	100147/10050
*R*int	0.1482	0.1167	0.1033
Data/restraints/parameters	10617/0/277	10826/0/277	10050/0/277
GOF on F^2	1.131	1.069	1.134
R_1[a], wR_2[b] [I > 2σ(I)]	0.0938, 0.2277	0.0488, 0.1386	0.0759, 0.2315
R_1[a], wR_2[b] (all data)	0.1165, 0.2444	0.0577, 0.1415	0.1116, 0.2736

[a] $R_1 = \Sigma||F_o|-|F_c||/\Sigma|F_o|$. [b] $wR_2 = [\Sigma w(F_o^2 - F_c^2)^2/\Sigma w(F_o^2)^2]^{1/2}$.

Table S2. Selected bond lengths (Å) of SNNU-5 analogue.

SNNU-5-Al			
Al(1)-O(1)	1.948(3)	Al(2)-O(2)	1.8922(19)
Al(1)-O(9)	1.826(3)	Al(2)-O(3)#4	1.8913(19)
Al(1)-O(8)#1	1.8802(18)	Al(2)-O(4)#5	1.9181(19)
Al(1)-O(8)#2	1.8800(18)	Al(2)-O(6)#1	1.9235(18)
Al(1)-O(5)#3	1.8947(17)	Al(2)-O(7)	1.931(2)
Al(1)-O(5)#4	1.8946(17)	Al(2)-O(9)	1.8302(13)

Symmetry codes: (#1) x-y, x, -z; (#2) x+1/3, x-y-1/3, z+1/6; (#3) -x+y+1, -x, z; (#4) -x+1/3, -x+y+2/3, -z+1/6; (#5) y+1/3, x-1/3, -z+1/6.

SNNU-5-Ga			
Ga(1)-O(1)	1.981(3)	Ga(2)-O(2)	1.9825(19)
Ga(1)-O(5)	1.9563(19)	Ga(2)-O(7)#2	1.9592(18)
Ga(1)-O(5)#1	1.9565(19)	Ga(2)-O(4)#4	1.9649(18)
Ga(1)-O(6)#2	1.9901(19)	Ga(2)-O(3)#5	2.0159(18)
Ga(1)-O(6)#3	1.9904(19)	Ga(2)-O(8)	2.0080(18)
Ga(1)-O(9)	1.875(3)	Ga(2)-O(9)	1.8744(12)

Symmetry codes: (#1) y-1/3, x+1/3, -z+5/6; (#2) -y+4/3, -x+5/3, z+1/6; (#3) -x+4/3, -y+5/3,-z+2/3, y+1/2; (#4) x-y+4/3, x+2/3, -z+2/3; (#5) x+1/3, x-y+5/3, z+1/6.

SNNU-5-In			
In(1)-O(1)	2.156(6)	In(2)-O(2)	2.170(7)
In(1)-O(3)	2.182(6)	In(2)-O(2)#1	2.170(7)
In(1)-O(5)	2.144(6)	In(2)-O(4)	2.143(7)
In(1)-O(6)#1	2.201(6)	In(2)-O(4)#1	2.143(7)
In(1)-O(7)	2.039(3)	In(2)-O(7)	2.039(7)
In(1)-O(8)	2.172(7)	In(2)-O(9)	2.152(11)

Symmetry codes: (#1) y+2/3,x-2/3,-z+5/6.

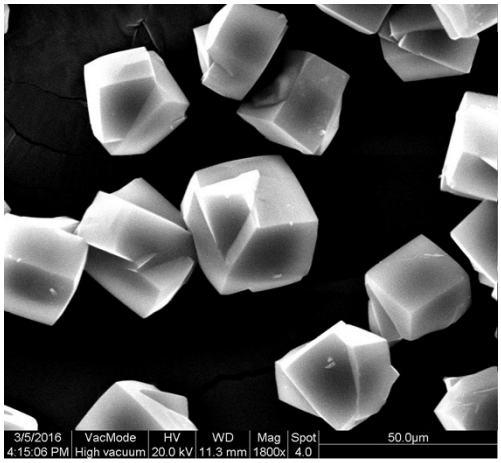

(a)

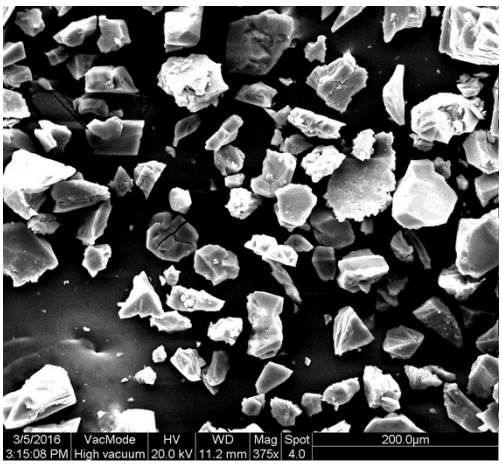

(b)

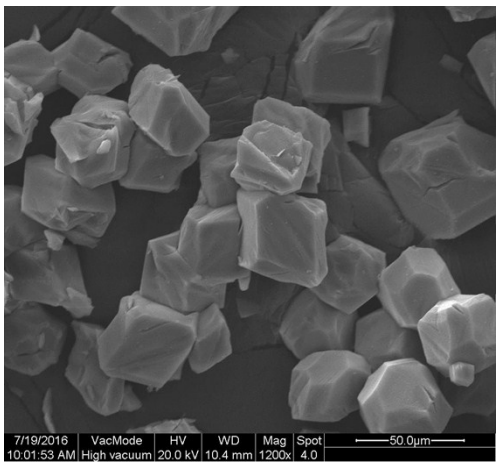

(c)

Figure S1. SEM photographs of SNNU-5 bulk MOF materials: SNNU-Al (a), SNNU-Ga (b) and SNNU-In (c).

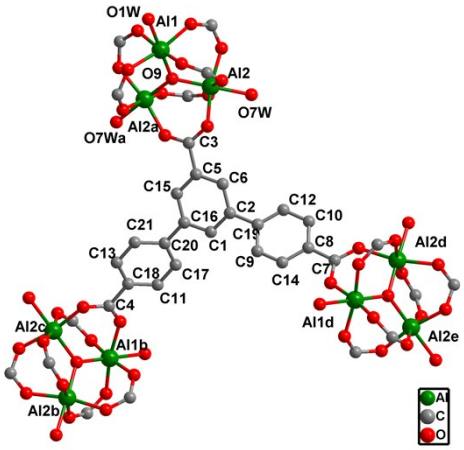

Figure S2. Description of the linkage between inorganic Al-trimer clusters and organic linker for SNNU-5-Al. (Symmetry codes: (a) 1/3+y, -1/3+x, 1/6-z; (b) -y, -1+x-y, z; (c) 1/3-x, -1/3-x+y, 1/6-z; (d) y, -x+y, -z; (e) -1/3+x, -2/3+x-y, -1/6+z.) (All the hydrogen atoms are omitted for clarity)

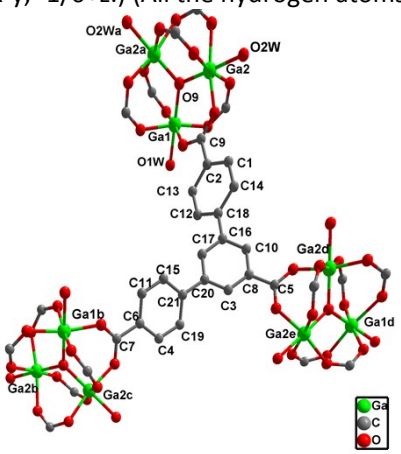

Figure S3. Description of the linkage between inorganic Ga-trimer clusters and organic linker for SNNU-5-Ga. (Symmetry codes: (a) -1/3+y, 1/3+x, 2/3-z; (b) 4/3-x, 5/3-y, 2/3-z; (c) 5/3-y, 4/3-x, -1/6+z; (d) -2/3+y, 2/3-x+y, 2/3-z; (e) -1/3+x, 4/3+x-y, -1/6+z.) (All the hydrogen atoms are omitted for clarity)

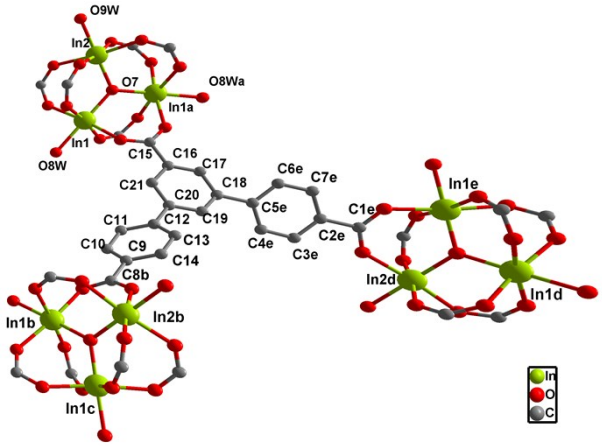

Figure S4. Description of the linkage between inorganic In-trimer clusters and organic linker for SNNU-5-In. (Symmetry codes: (a) 2/3+y, -2/3+x, 5/6-z; (b) 1/3+x-y, -1/3+x, 2/3-z; (c) 5/3-x+y, 1/3+y, -1/6+z; (d) 2-x+y, 1-x, z; (e) 2/3+x-y, 1/3-y, 5/6-z.) (All the hydrogen atoms are omitted for clarity)

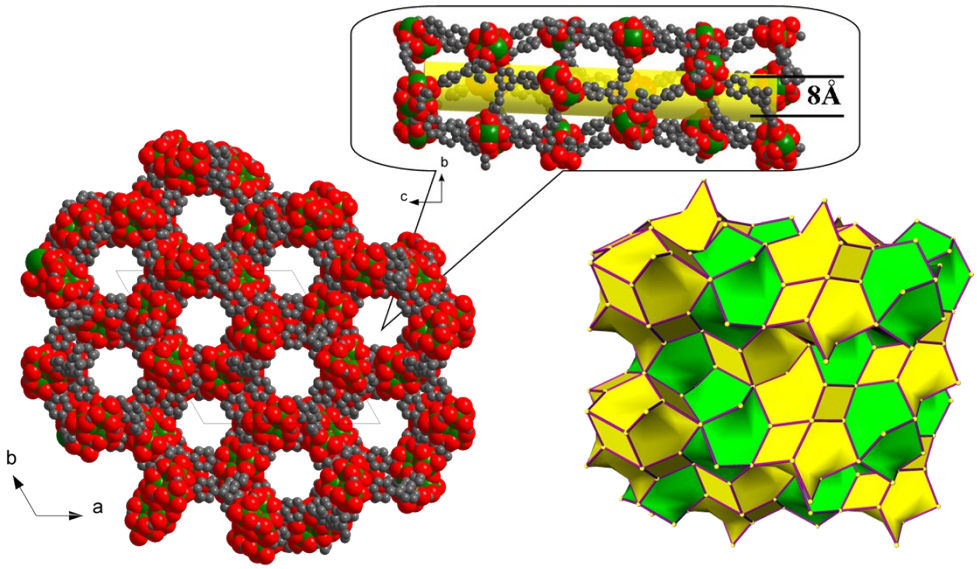

Figure S5. Space-filling diagram of the framework showing 1 D channels along *c*-axis and complete tiling representation of SNNU-5s (Guest molecules and H atoms have been omitted for clarity.)

Topology Analysis of SNNU-5s

To better understand the framework topology, each μ_3-O trinuclear unit can be defined as a 6-connected node with trigonal-prismatic geometry, while the tritopic DCPB ligand can be simplified as a 3-connected node having triangle geometry (Figure S). As a result, the whole structure of SNNU-5s exhibits a (3, 6)-connected dinodal net as of a new topology:

Point symbol for net: $\{4.6^2\}_2\{4^2.6^7.8^6\}$

TD10 = 1333

Topological terms for each node:

(V1 for DCPB ligand) Point symbol: $\{4.6^2\}$

Extended point symbol: [4.6(2).6(2)]

Coordination sequence: 3 14 19 62 56 157 113 288 189 454

(V2 for μ_3-O trimer) Point symbol: $\{4^2.6^7.8^6\}$

Extended point symbol: [4.4.6.6.6.6.6.6.6(2).8(2).8(3).8(3).8(3).8(3).8(6)]

Coordination sequence: 6 10 38 38 112 86 226 154 378 238

Transitivity: [2332]

Tilling: $[6^8]$ + $[4^6.6^8]$

Topological type: New topology

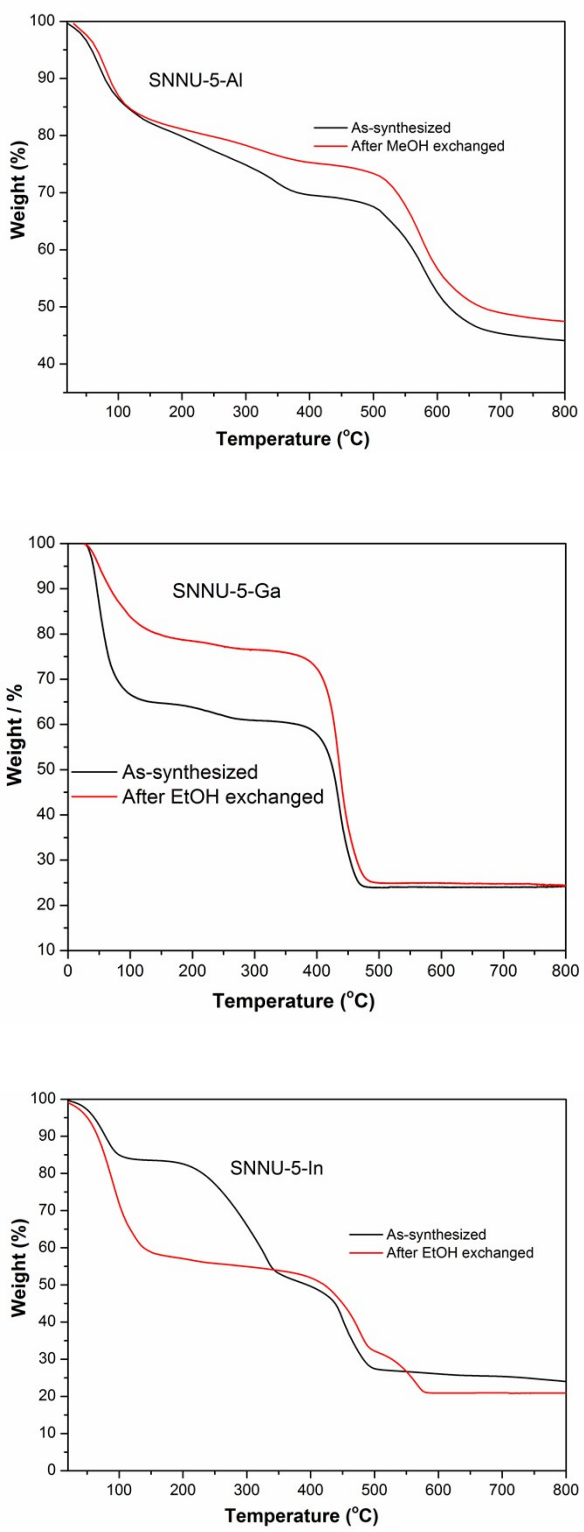

Figure S6. TGA curves for the as-synthesized and exchanged samples of SNNU-5-Al/Ga/In.

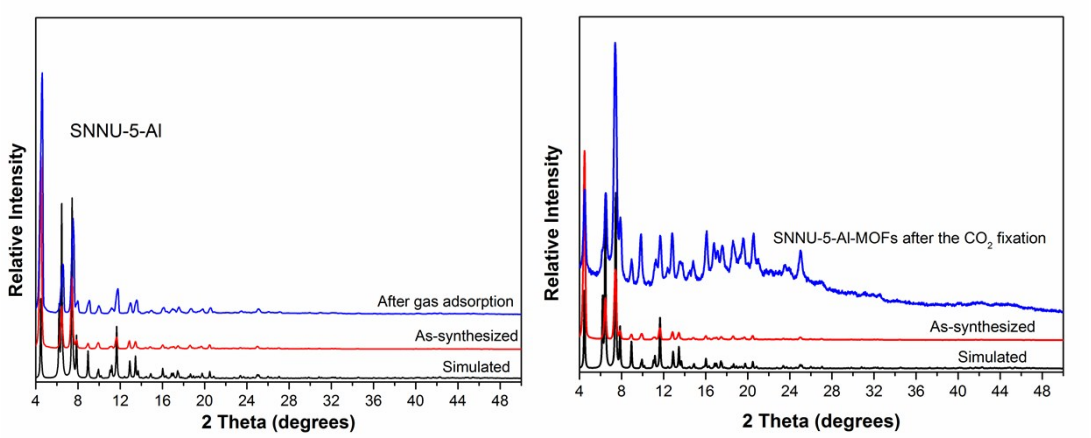

Figure S7. PXRD patterns of SNNU-5-Al by various treatments.

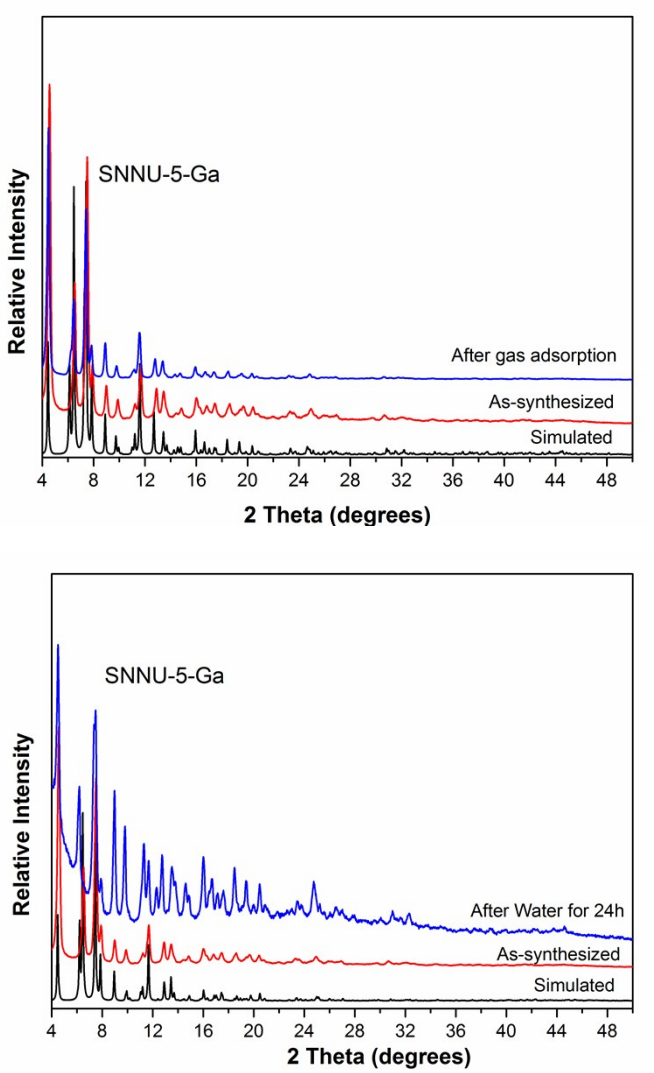

Figure S8. PXRD patterns of SNNU-5-Ga by various treatments.

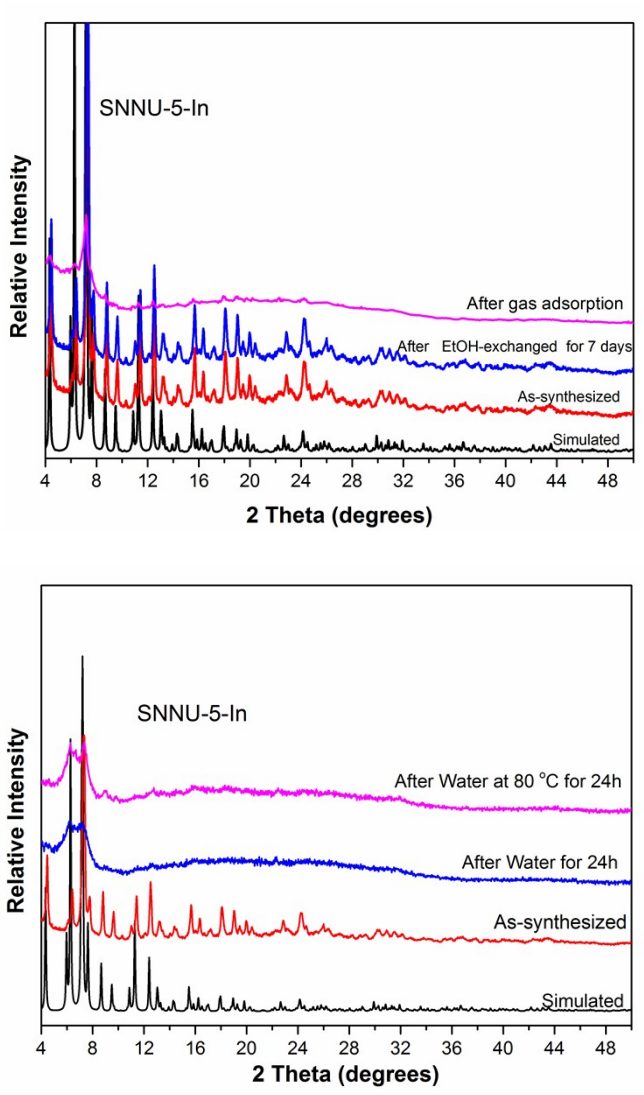

Figure S9. PXRD patterns of SNNU-5-In by various treatments.

Estimation of the Isosteric Heats of Gas Adsorption

To extract the coverage-dependent isosteric heat of adsorption for compounds, the data were modeled with a virial-type expression[S1] composed of parameters a_i and b_i that are independent of temperature:

$$\ln P = \ln N + \frac{1}{T}\sum_{i=0}^{m} a_i N^i + \sum_{i=0}^{n} b_i N^i \qquad (1)$$

$$Q_{st} = -R\sum_{i=0}^{m} a_i N^i \qquad (2)$$

Where P is pressure, N is the amount adsorbed (or uptake), T is temperature, and m and n determine the number of terms required to adequately describe the isotherm. R is the universal gas constant. The coverage dependencies of Q_{st} calculated from fitting the data at 273 K and 298 K under the pressure range from 0-1 bar, and Q_{st} and R is the universal gas constant.

Selectivity Prediction for Binary Mixture Adsorption

Ideal adsorbed solution theory (IAST)[S2,S3] was used to predict binary mixture adsorption from the experimental pure-gas isotherms. To perform the integrations required by IAST, the single-component isotherms should be fitted by a proper model. The Dual-Site Langmuir–Freundlich (DSLF) equation was found to the best fit to the experimental pure isotherms for CO_2, C_2H_2, and C_2H_4 and CH_4 of SNNU-5 analogue. On the base of the equation parameters of pure gas adsorption, the IAST model was further used to investigate the separation of CO_2/CH_4, C_2H_2/CH_4, C_2H_4/CH_4. C_2H_2/CO_2, C_2H_2/C_2H_4 and C_2H_4/CO_2.

$$q = q_{m1} * \frac{b_1 * p^{1/n_1}}{1 + b_1 * p^{1/n_1}} + q_{m2} * \frac{b_2 * p^{1/n_2}}{1 + b_2 * p^{1/n_2}}$$

where p is the pressure of the bulk gas at equilibrium with the adsorbed phase (kPa), q is the adsorbed amount per mass of adsorbent (mmol g^{-1}), q_{m1} and q_{m2} are the saturation capacities of site 1 and 2 (mmol g^{-1}), b_1 and b_2 are the affinity coefficients of site (1/kPa), and n_1 and n_2 represent the deviations from an ideal homogeneous surface. The correlation coefficients (R^2) values for all of the fitted isotherms were over 0.9999. Hence, the fitted isotherm parameters were applied to perform the necessary integrations in IAST.

Based on the above equation parameters of pure gas adsorption, we used the IAST model to investigate the separation performance of SNNU-5 MOFs. The adsorption selectivity is defined by

$$s_{A/B} = \frac{x_A / y_A}{x_B / y_B}$$

Where x_i and y_i are the mole fractions of component i (i = A, B) in the adsorbed and bulk phases, respectively. Note that in the Henry regime $S_{A/B}$ is identical to the ratio of the Henry constants of the two species.

Table S3. Summary of gas sorption properties for SNNU-5s.

MOFs	SNNU-5-Al	SNNU-5-Ga	SNNU-5-In
S_A Langmuir ($m^2 g^{-1}$)	3248.4	2791.6	2945.0
S_A BET ($m^2 g^{-1}$)	2077.8	1781.7	1876.7
Pore volume ($cm^3 g^{-1}$)	1.13	0.97	1.03
Pore size (Å)	6.8	6.9	7.1
H_2 77 K, 1 atm ($cm^3 g^{-1}$/wt%)	324.4/2.9	255.2/2.3	200.8/1.8
CO_2 273 K, 1 atm ($cm^3 g^{-1}$)	121.4	102.6	72.7
CO_2 298 K, 1 atm ($cm^3 g^{-1}$)	67.9	53.7	36.2
Q_{st} (kJ/mol) for CO_2	19.6	20.9	31.9
C_2H_2 273 K, 1 atm ($cm^3 g^{-1}$)	216.0	171.2	155.4
C_2H_2 298 K, 1 atm ($cm^3 g^{-1}$)	144.2	102.2	76.6
Q_{st} (kJ/mol) for C_2H_2	25.5	39.9	28.9
C_2H_4 273 K, 1 atm ($cm^3 g^{-1}$)	159.9	135.7	120.4
C_2H_4 298 K, 1 atm ($cm^3 g^{-1}$)	97.3	81.1	66.4
Q_{st} (kJ/mol) for C_2H_4	19.5	21.0	18.1
CH_4 273 K, 1 atm ($cm^3 g^{-1}$)	27.8	21.7	18.3
CH_4 298 K, 1 atm ($cm^3 g^{-1}$)	17.5	13.1	11.2
Q_{st} (kJ/mol) for CH_4	10.2	13.9	12.3

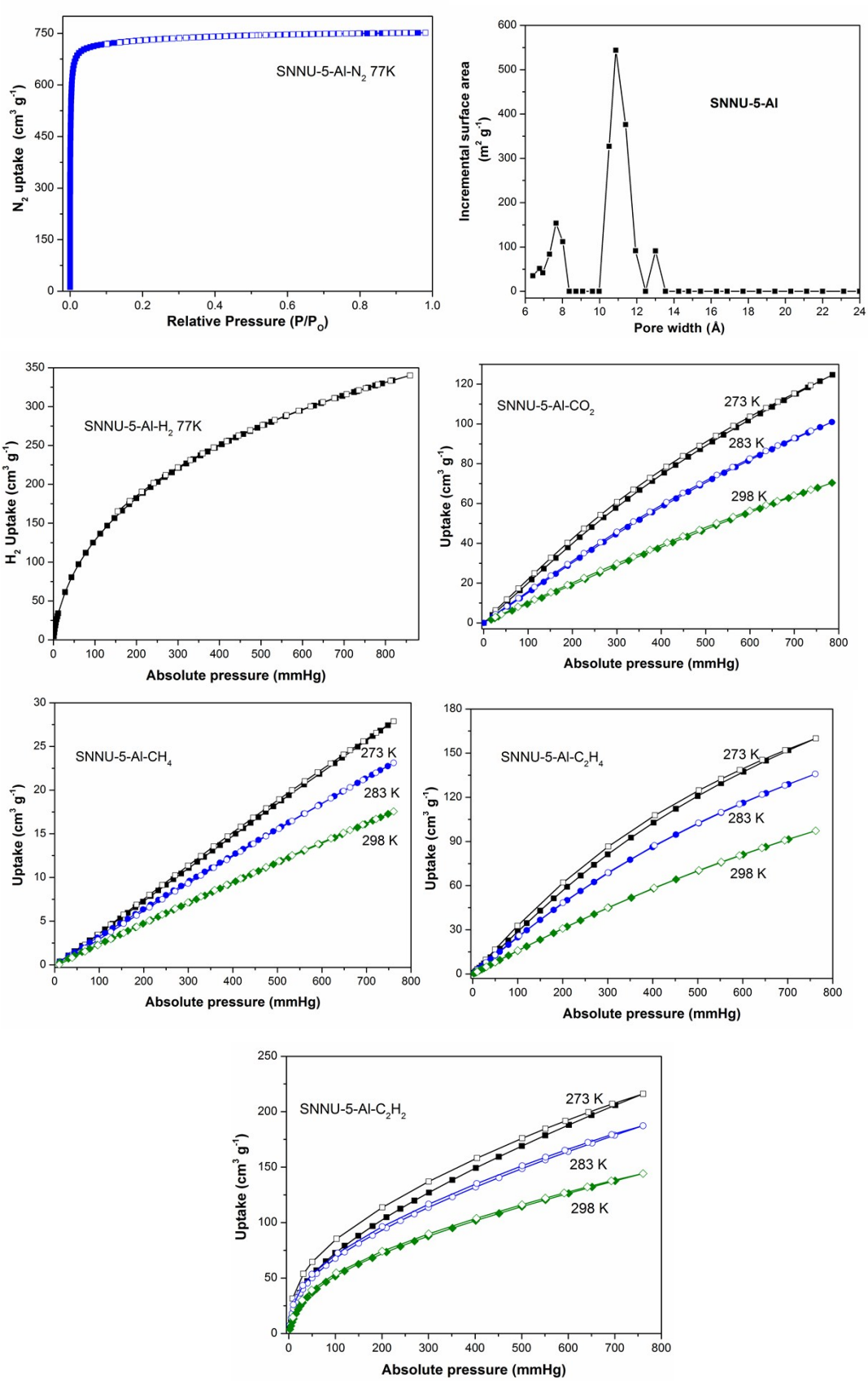

Figure S10. N_2, H_2, CO_2, CH_4, C_2H_4 and C_2H_2 adsorption and desorption isotherms for SNNU-5-Al (Solid and open symbols indicate adsorption and desorption isotherms, respectively.)

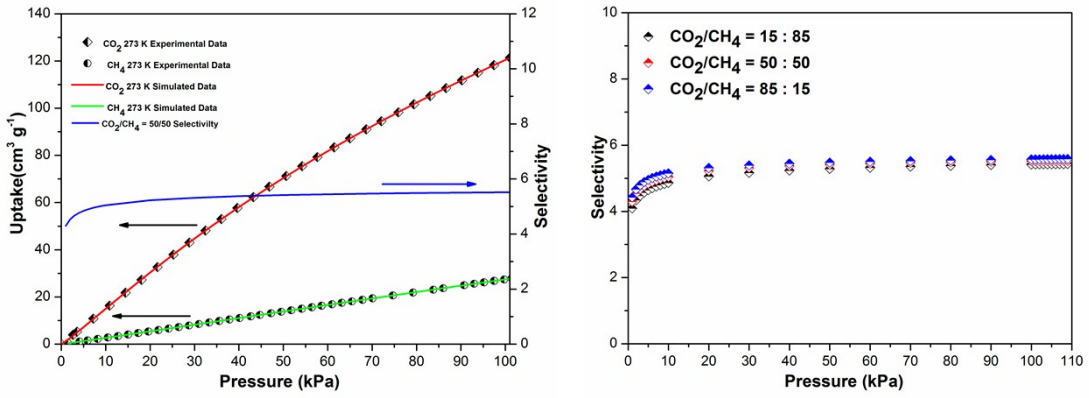

(a)

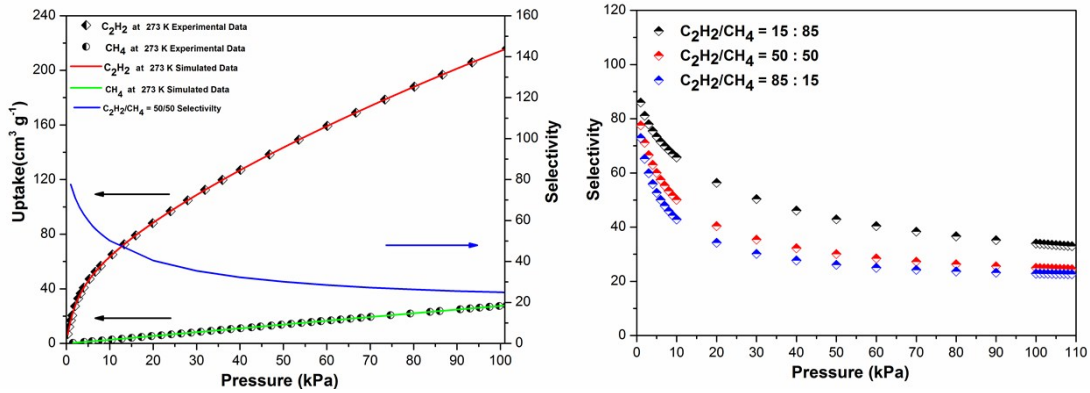

(b)

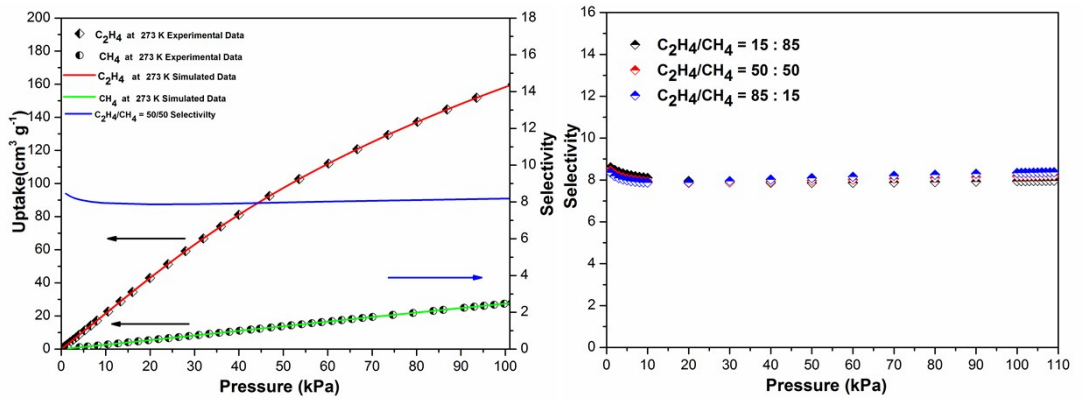

(c)

Figure S11. Comparison of experimental isotherms and simulated isotherms (Left *Y* axis), and mixture adsorption selectivity predicted for equimolar binary-mixture and three different composition selectivity predicted by IAST (Right *Y* axis) of SNNU-5-Al for binary mixture at 273 K: (a) CO_2/CH_4, (b) C_2H_2/CH_4 and (c) C_2H_4/CH_4.

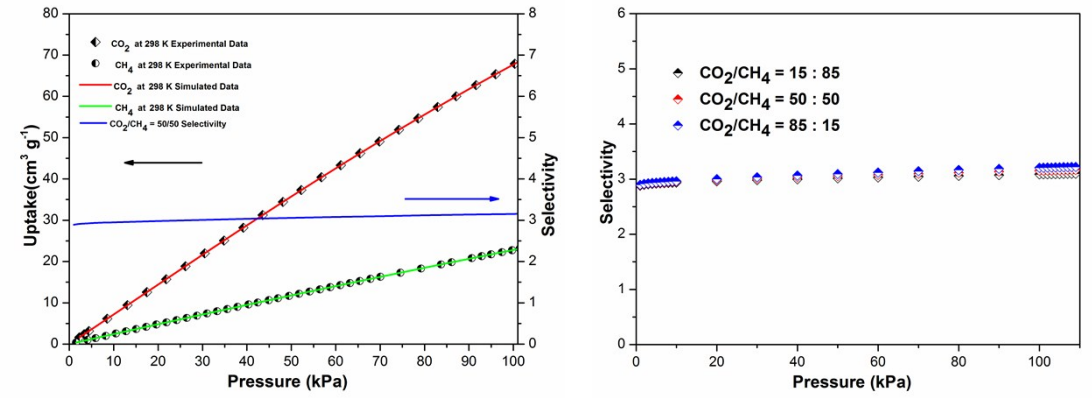

(a)

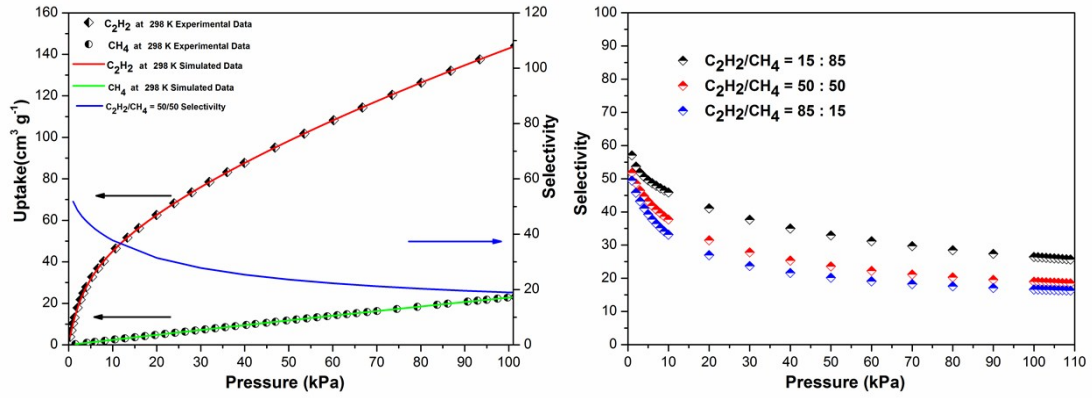

(b)

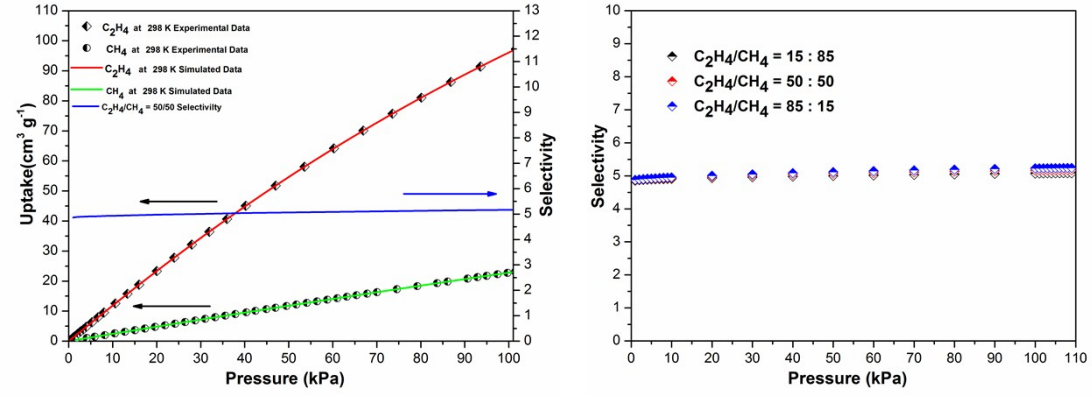

(c)

Figure S12. Comparison of experimental isotherms and simulated isotherms (Left *Y* axis), and mixture adsorption selectivity predicted for equimolar binary-mixture and three different composition selectivity predicted by IAST (Right *Y* axis) of SNNU-5-Al for binary mixture at 298 K: (a) CO_2/CH_4, (b) C_2H_2/CH_4 and (c) C_2H_4/CH_4.

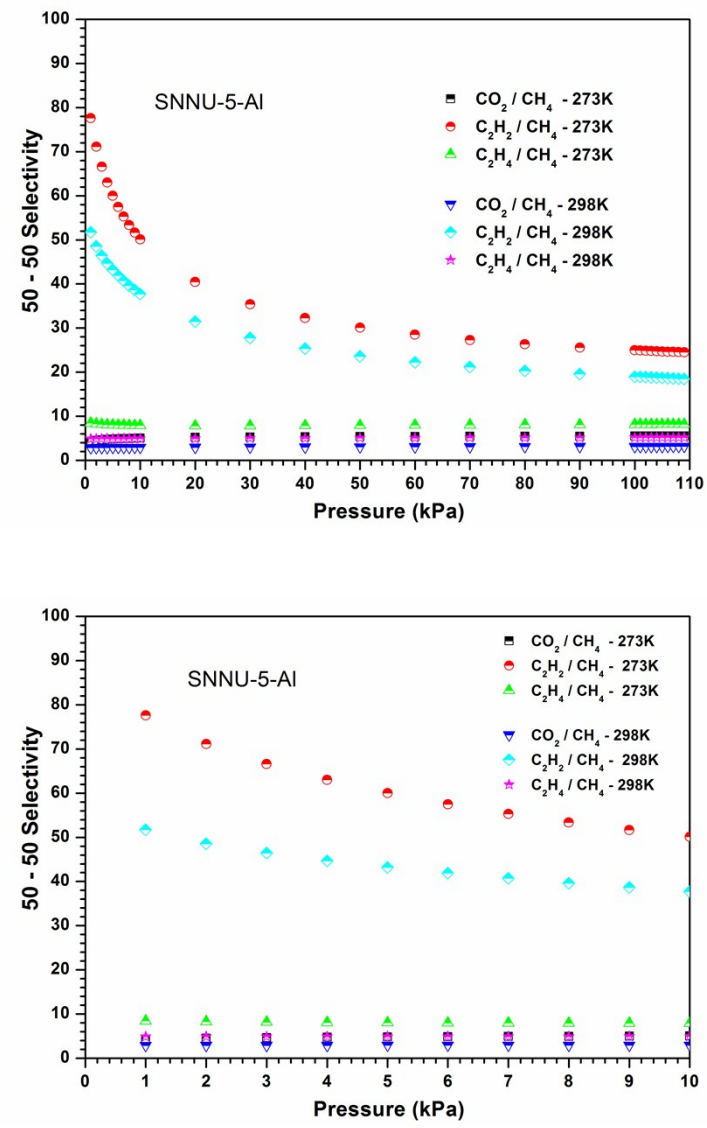

Figure S13. Comparison of selectivity predicted for an equimolar binary-mixture at 273 and 298 K (up to 10 and 110 kPa, respectively) by IAST for SNNU-5-Al.

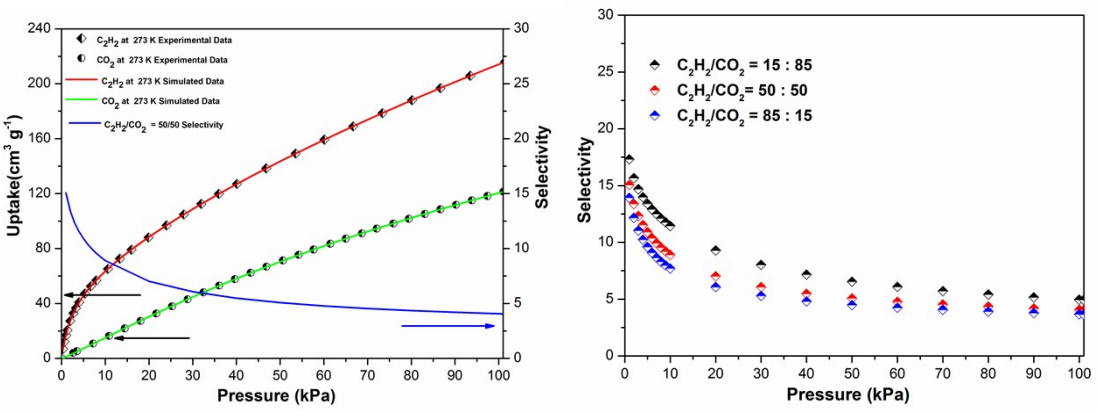

(a)

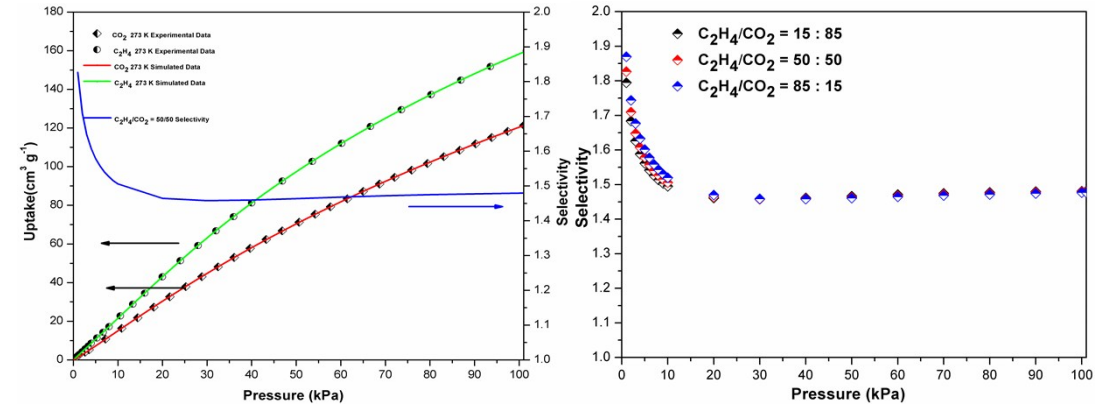

(b)

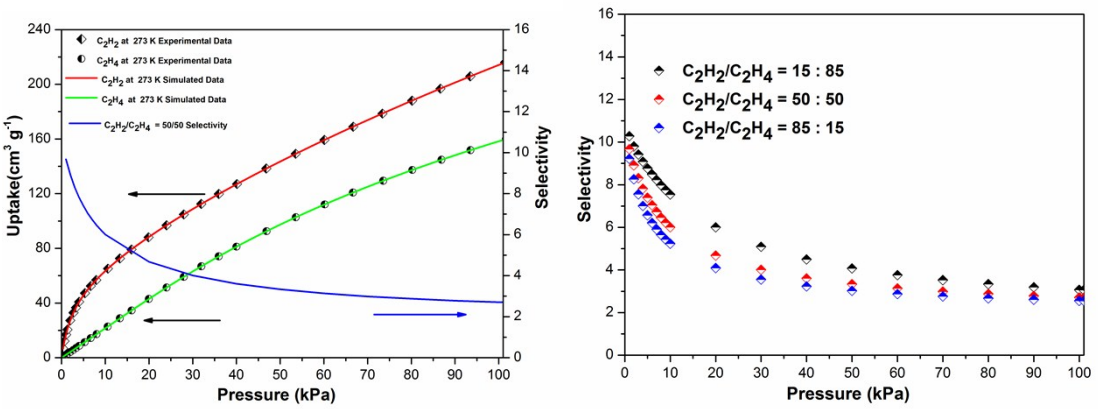

(c)

Figure S14. Comparison of experimental isotherms and simulated isotherms (Left *Y* axis), and mixture adsorption selectivity predicted for equimolar binary-mixture and three different composition selectivity predicted by IAST (Right *Y* axis) of SNNU-5-Al for binary mixture at 273 K: (a) C_2H_2/ CO_2, (b) C_2H_4/ CO_2 and (c) C_2H_2/ C_2H_4.

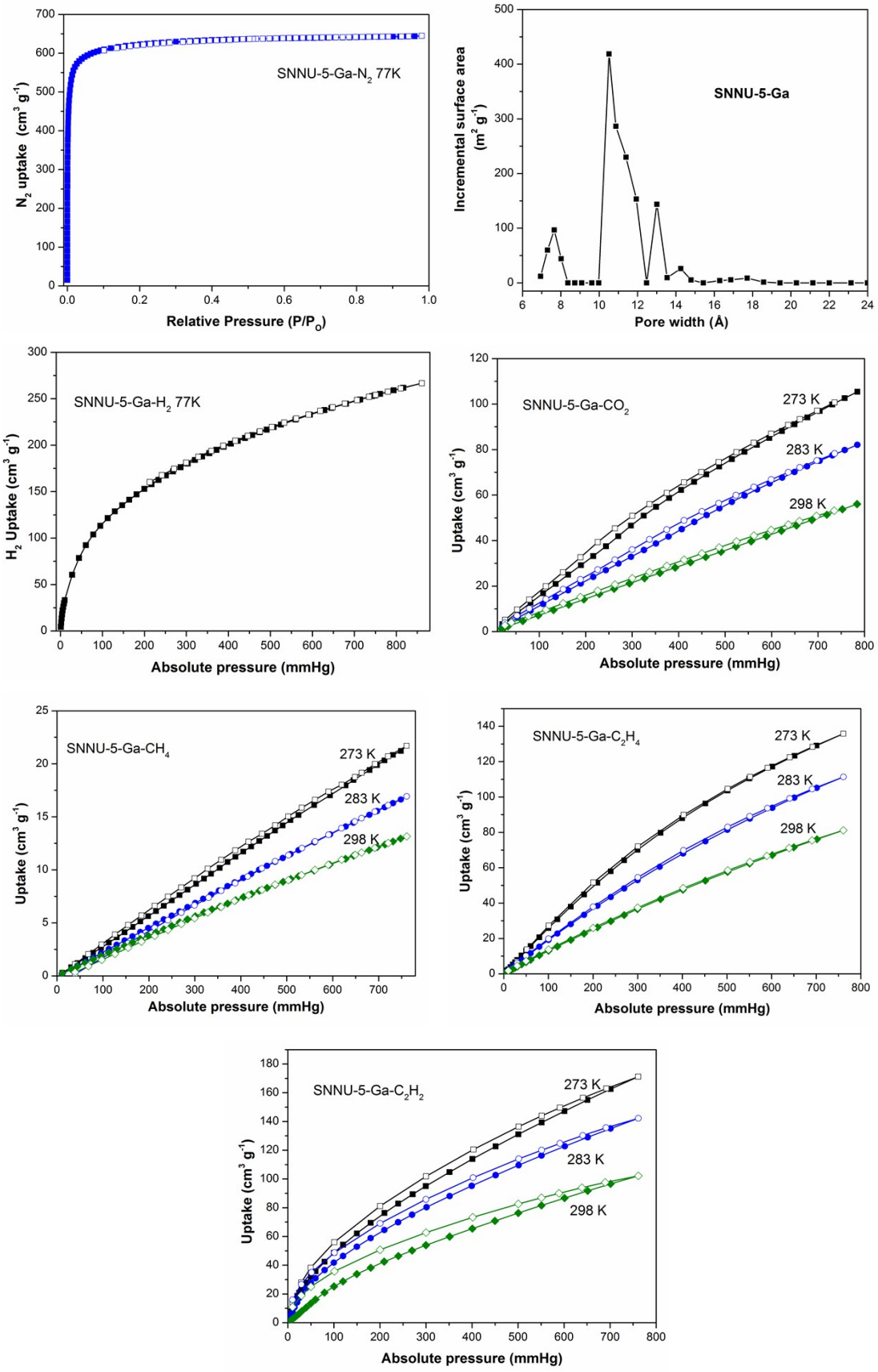

Figure S15. N_2, H_2, CO_2, CH_4, C_2H_4 and C_2H_2 adsorption and desorption isotherms for SNNU-5-Ga (Solid and open symbols indicate adsorption and desorption isotherms, respectively.)

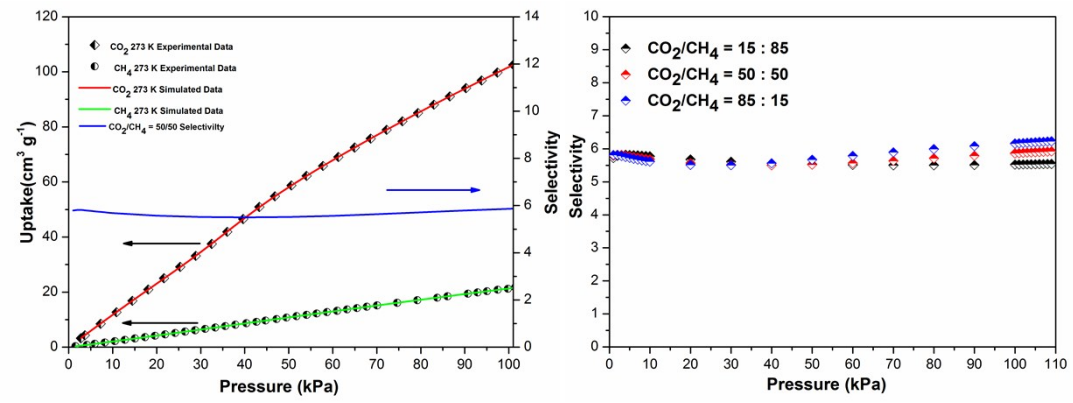

(a)

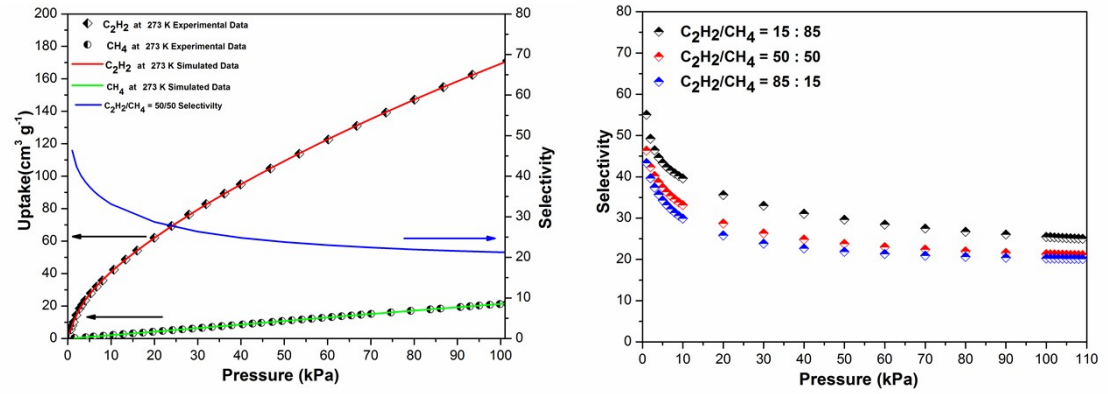

(b)

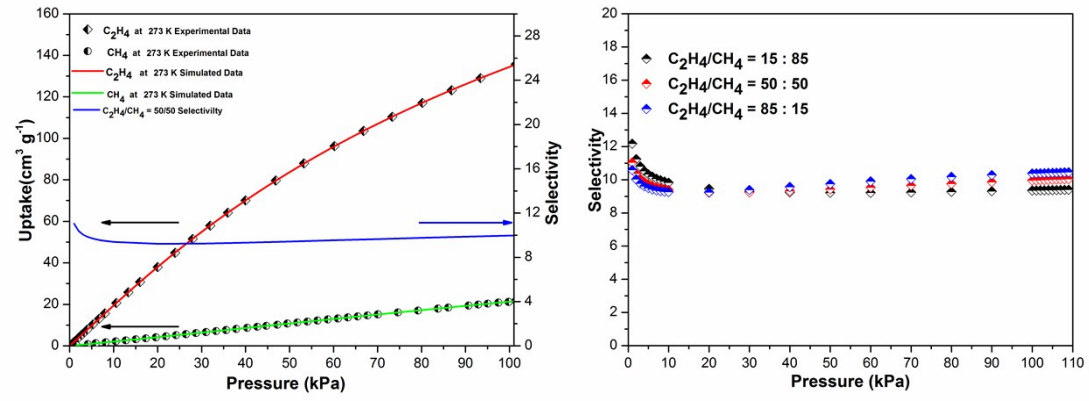

(c)

Figure S16. Comparison of experimental isotherms and simulated isotherms (Left *Y* axis), and mixture adsorption selectivity predicted for equimolar binary-mixture and three different composition selectivity predicted by IAST (Right *Y* axis) of SNNU-5-Ga for binary mixture at 273 K: (a) CO_2/CH_4, (b) C_2H_2/CH_4 and (c) C_2H_4/CH_4.

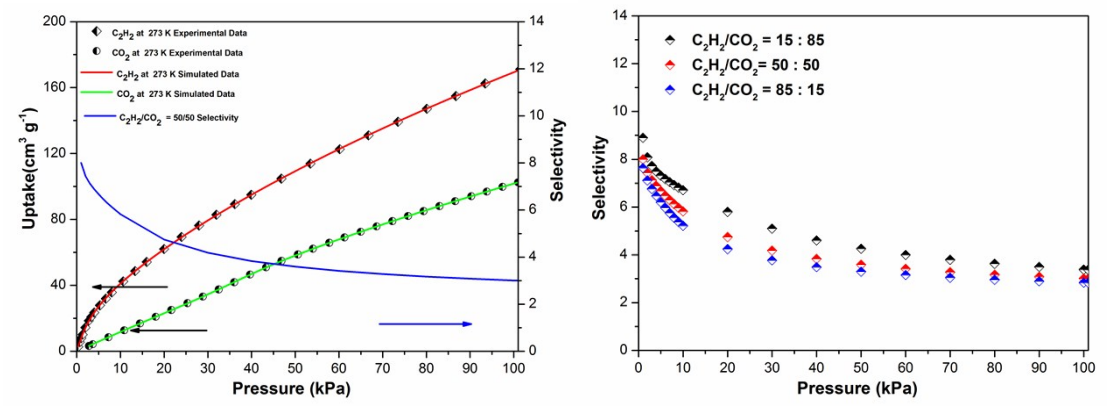

(a)

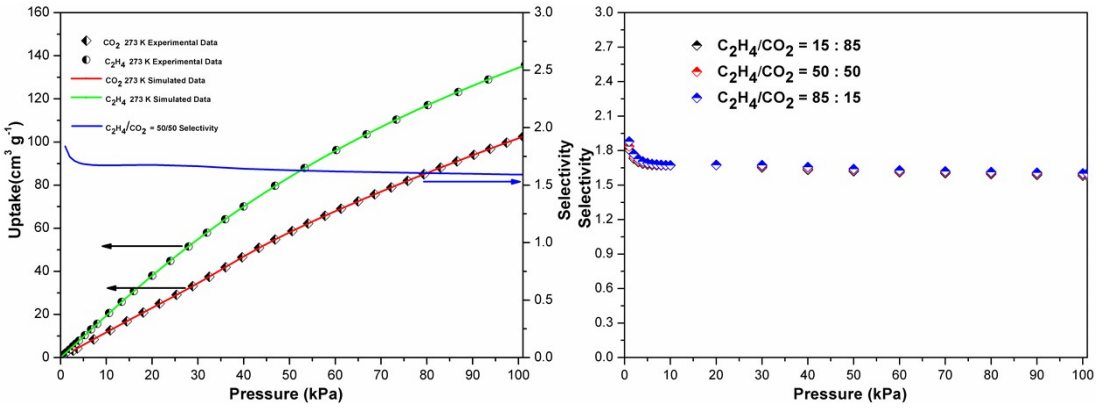

(b)

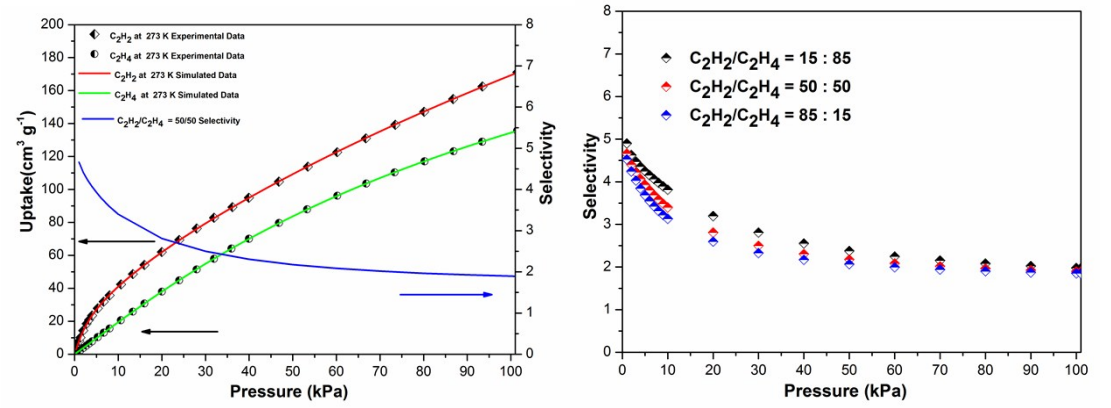

(c)

Figure S17. Comparison of experimental isotherms and simulated isotherms (Left *Y* axis), and mixture adsorption selectivity predicted for equimolar binary-mixture and three different composition selectivity predicted by IAST (Right *Y* axis) of SNNU-5-Ga for binary mixture at 273 K: (a) C_2H_2/ CO_2, (b) C_2H_4/ CO_2 and (c) C_2H_2/ C_2H_4.

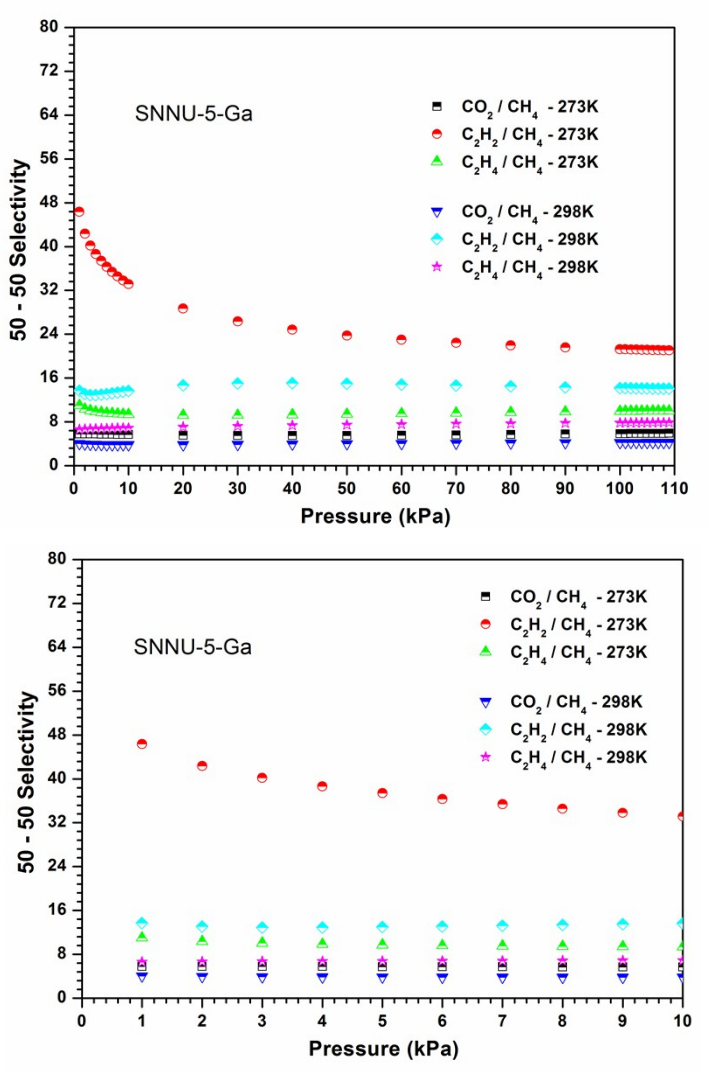

Figure S18. The comparison of selectivity predicted for an equimolar binary-mixture at 273 and 298 K (up to 10 and 110 kPa, respectively) by IAST for SNNU-5-Ga.

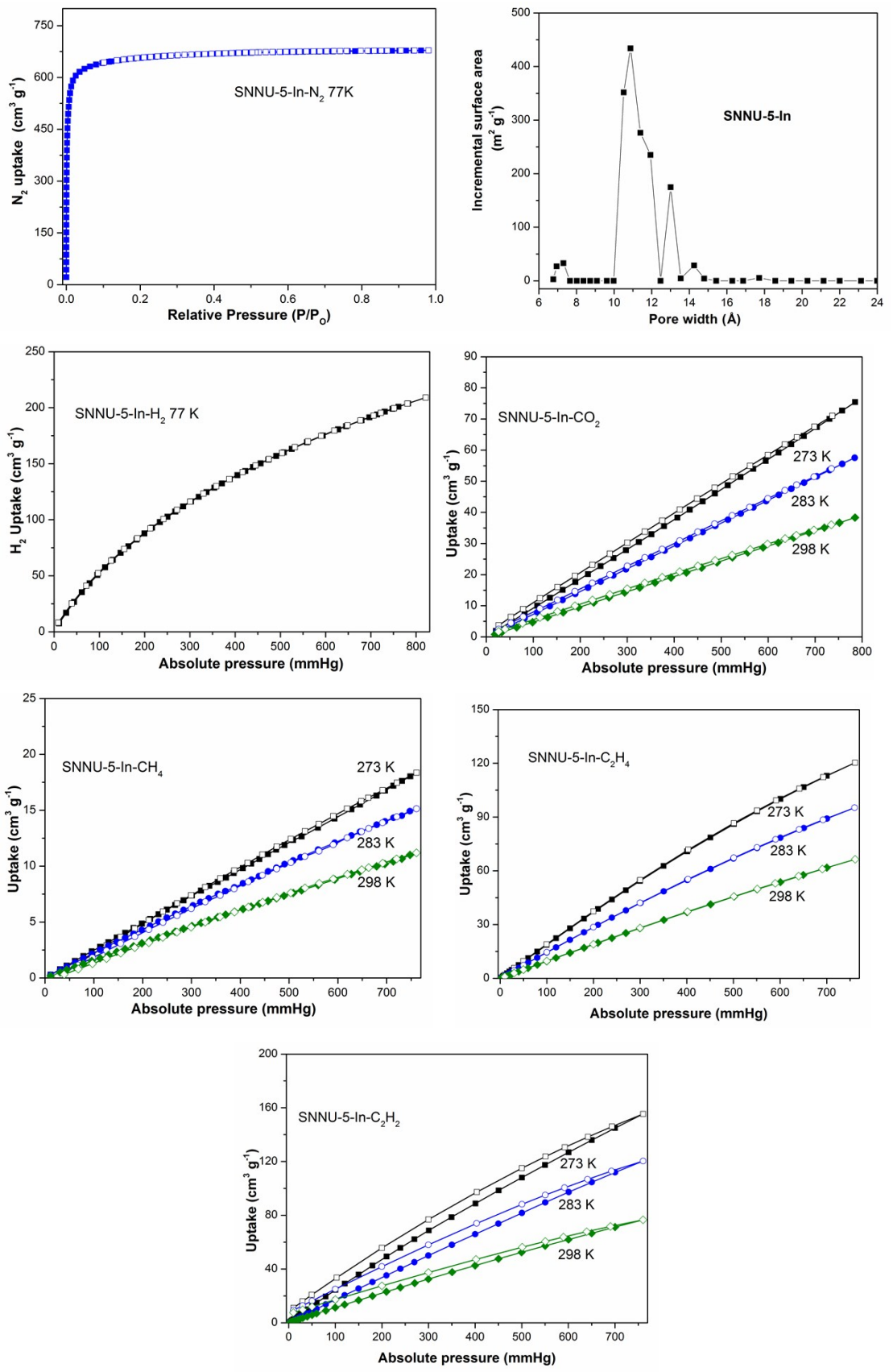

Figure S19. N_2, H_2, CO_2, CH_4, C_2H_4 and C_2H_2 adsorption and desorption isotherms for SNNU-5-In (Solid and open symbols indicate adsorption and desorption isotherms, respectively.

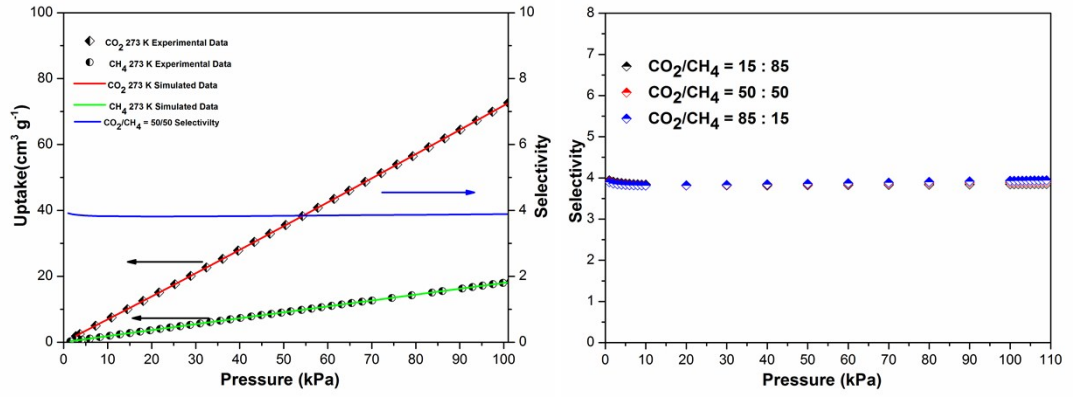

(a)

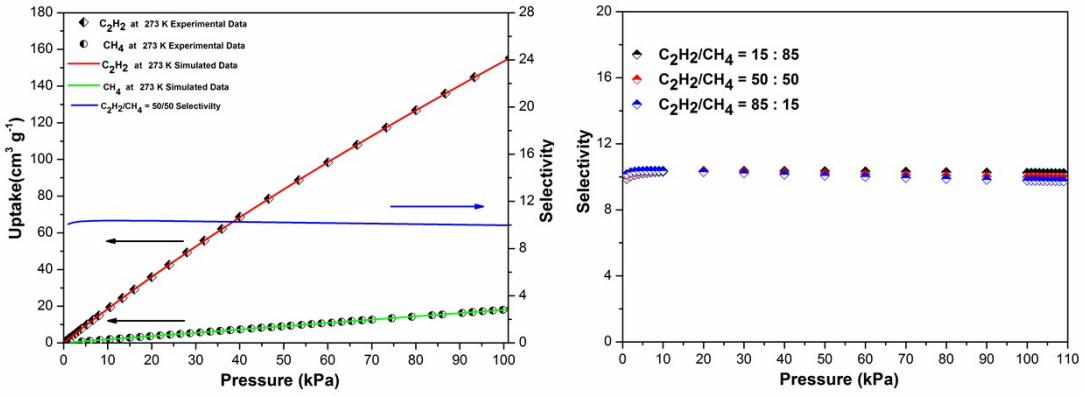

(b)

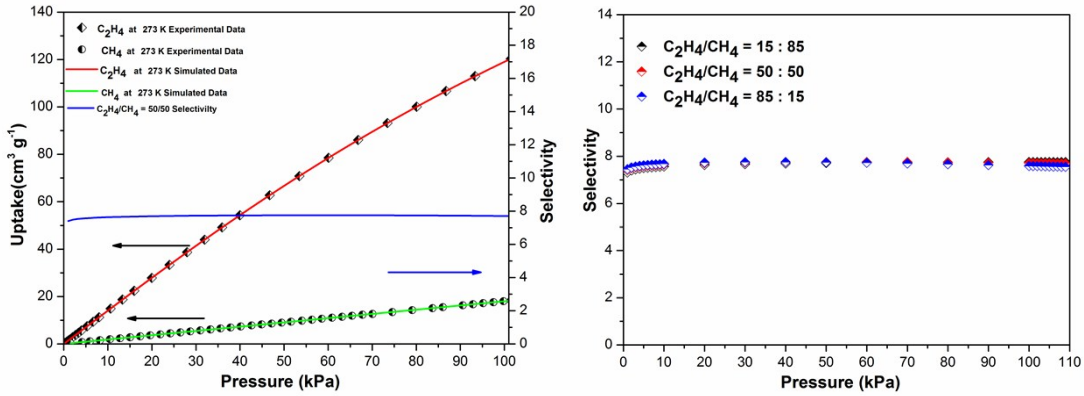

(c)

Figure S20. Comparison of experimental isotherms and simulated isotherms (Left *Y* axis), and mixture adsorption selectivity predicted for equimolar binary-mixture and three different composition selectivity predicted by IAST (Right *Y* axis) of SNNU-5-In for binary mixture at 273 K: (a) CO_2/CH_4, (b) C_2H_2/CH_4 and (c) C_2H_4/CH_4.

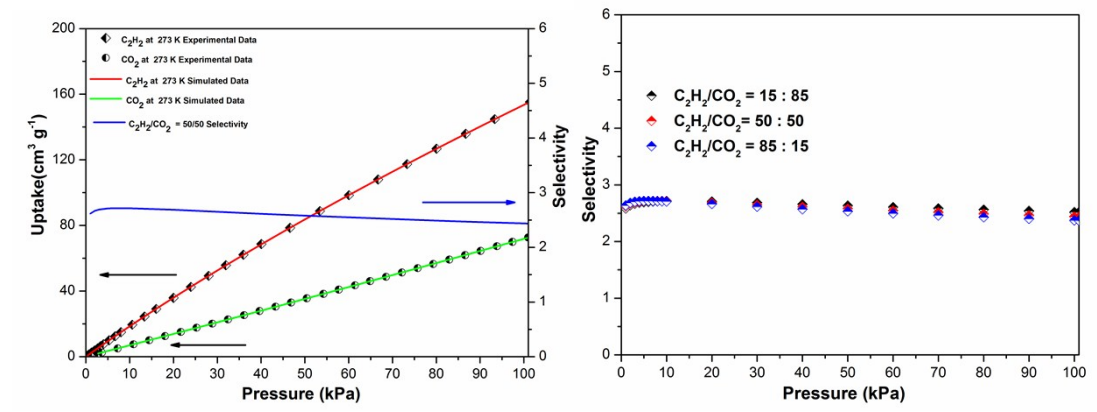

(a)

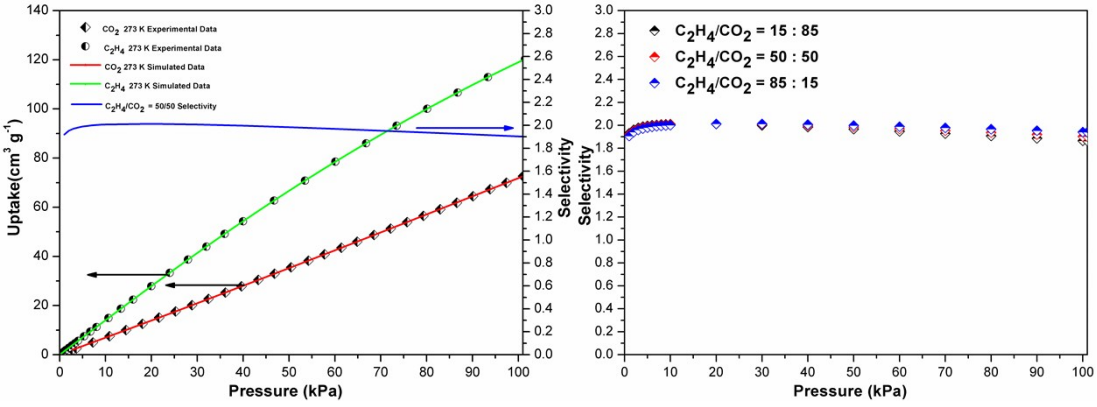

(b)

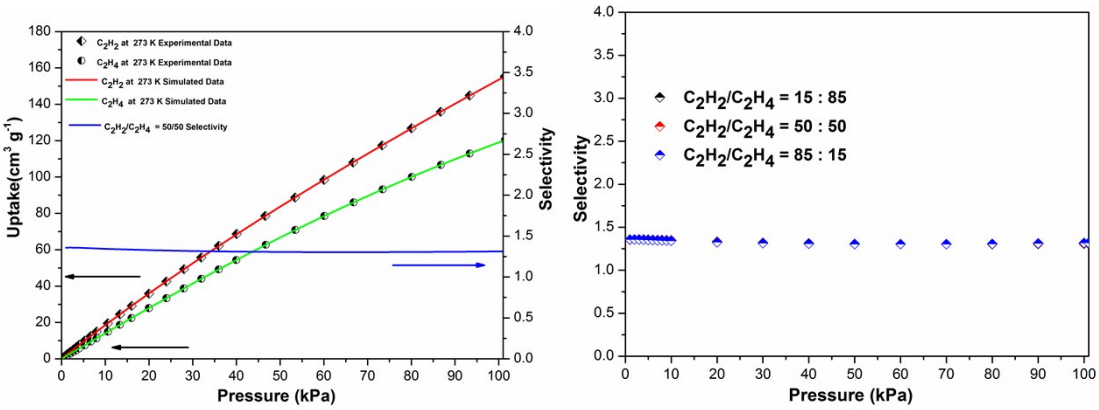

(c)

Figure S21. Comparison of experimental isotherms and simulated isotherms (Left *Y* axis), and mixture adsorption selectivity predicted for equimolar binary-mixture and three different composition selectivity predicted by IAST (Right *Y* axis) of SNNU-5-In for binary mixture at 273 K: (a) C_2H_2/CO_2, (b) C_2H_4/CO_2 and (c) C_2H_2/C_2H_4.

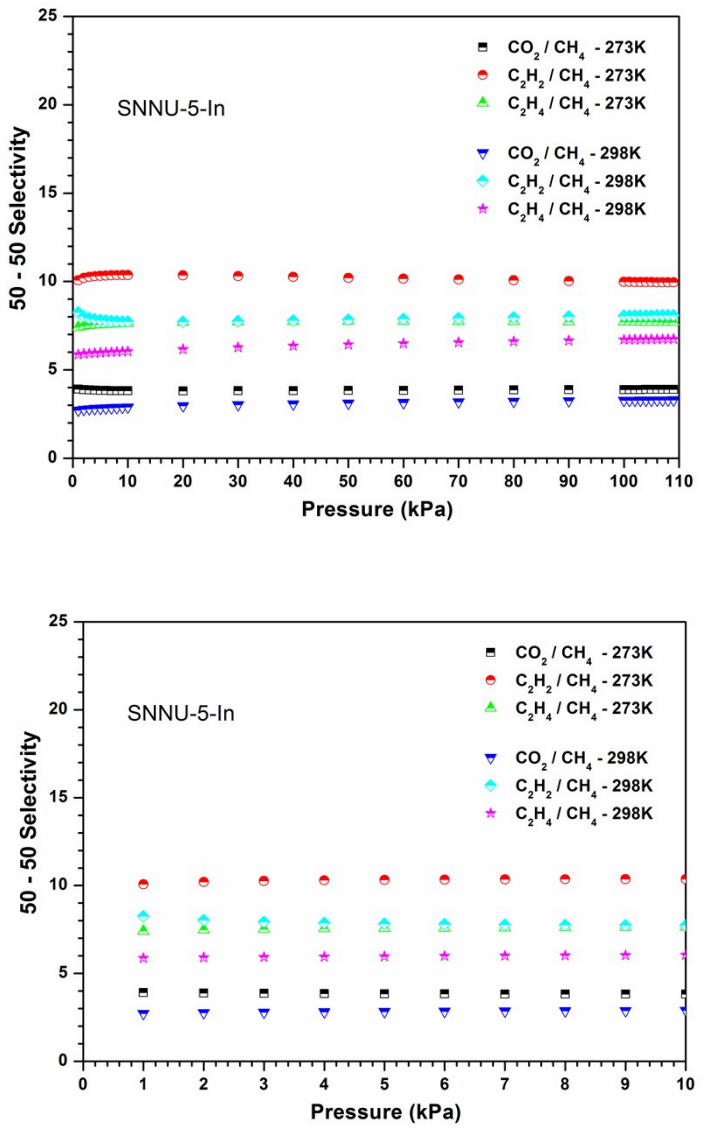

Figure S22. Comparison of selectivity predicted for an equimolar binary-mixture at 273 and 298 K (up to 10 and 110 kPa, respectively) by IAST for SNNU-5-In.

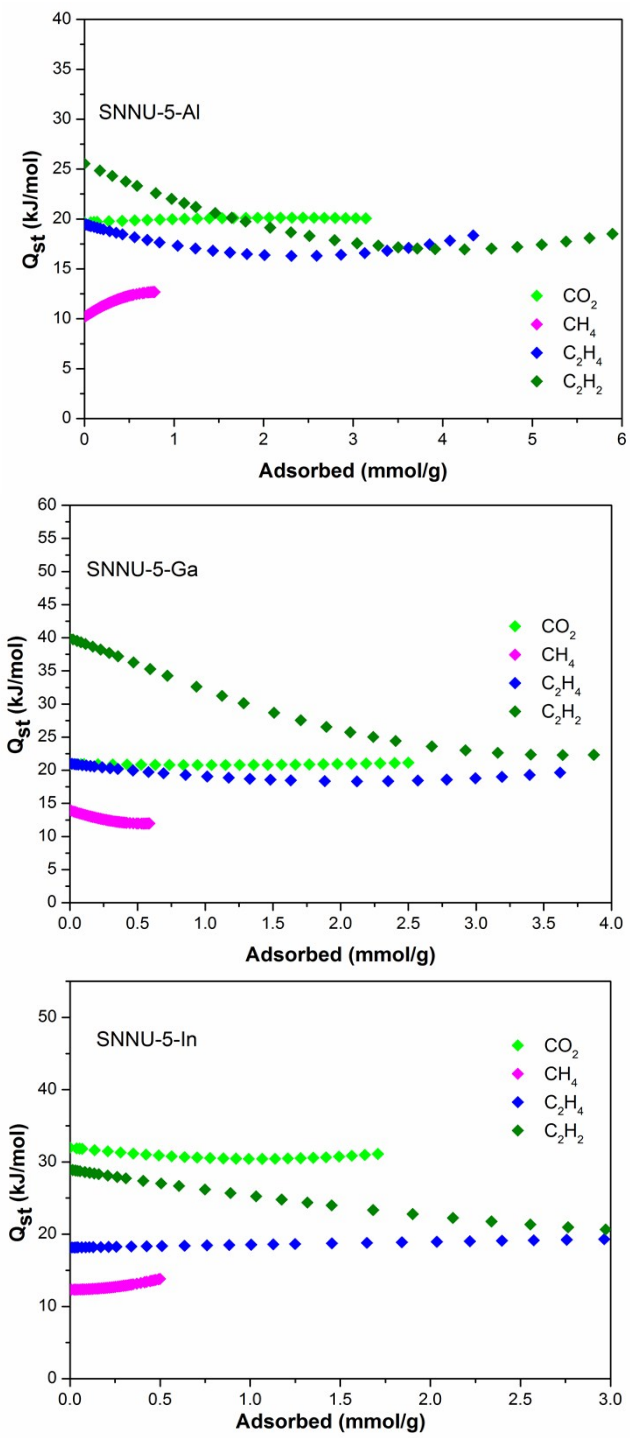

Figure S23. Comparisons of the isosteric heats of adsorption (Q_{st}) with low loading for SNNU-5s.

Table S4 Summary of top-high total methane uptakes and volumetric working capacity for MOFs based on high valent (+3 and +4) metals.

MOF	BET ($m^2 g^{-1}$)	*V*p ($cm^3 g^{-1}$)	*D*c ($g\ cm^{-3}$)	35 bar ($cm^3 g^{-1}$)/ ($cm^3 cm^{-3}$)	65 bar, ($cm^3 g^{-1}$)/ ($cm^3 cm^{-3}$)	working capacity at 35 bar ($cm^3 cm^{-3}$)	working capacity at 65 bar ($cm^3 cm^{-3}$)	T (K)	Ref.
SNNU-5-Al	2077.8	1.13	0.557	234/130	279/155	91	116	298	This work
MOF-519-Al	2400	0.938	0.953	210/200	297/279 at 80 bar	151	230	298	[S4]
MOF-520-Al	3290	1.277	0.586	276/ 162	399/ 231	125	194	298	[S4]
Al-soc-MOF-1	5585	2.3	0.34	361/123	579/196.9	-	176	298	[S5]
MIL-53-Al	1235	0.54	0.978	190/186	-	-	-	303	[S6]
DUT-5 (Al)	1613	0.81	0.634	-/114	-/160	94	137	298	[S7]
DUT-4 (Al)	1308	0.68	0.773	-/122	-/164	82	124	303	[S7]
MIL-101c(Cr)	4230	2.15	0.44	295/130	450/198	104	172	303	[S8]
MIL-100(Cr)	1900	1.1	0.7	205/144	288/202	114	172	303	[S8]
MIL-53(Cr)	1.04	-	1.017	-/165	-	-	-	304	[S9]
PCN-250(Fe_2Co)	-	-	0.953	-/200	-	-	-	298	[S10]
MIL-100(Fe)	2410	0.99	0.7	167/117	225/158	92	133	303	[S11]
NU-1100(Zr)	4020	1.53	0.467	-	385/180	-	160	298	[S12]
DUT-51(Zr)	2335	1.08	0.655	-/118	-/161	87	130	298	[S13]
MIL-125(Ti)	1820	0.67	0.81	-/141	-	-	-	300	[S11]
UiO-66(Zr)	970	0.36	1.32	-/146	-	-	-	303	[S11]

Table S5 Cycloaddition of CO_2 and epoxides catalyzed by SNNU-5 MOFs under various conditions.

Entry	R	Catalyst	Yield (%)[d]	TON[e]	TOF (h^{-1})[f]
1[a]	Me	TBAB	23.6	-	-
2[a]	Me	Al-MOF	5.7	19.6	3.92
3[b]	Me	Al-MOF, TBAB	10.9	37.6	5.4
4[c]	Me	Al-MOF, TBAB	61.0	210.3	42.0
5[a]	Me	Al-MOF, TBAB	72.8	251.0	50.2
6[a]	CH_2Cl	Al-MOF, TBAB	90.7	312.7	62.5
7[a]	Ph	Al-MOF, TBAB	72.0	248.2	49.6
8[a]	$PhOCH_2$	Al-MOF, TBAB	32.0	110.3	22.1
9[a]	Me	Ga-MOF, TBAB	90.6	312.4	62.5
10[a]	Me	In-MOF, TBAB	97.0	334.5	66.9

a Unless otherwise noted all reactions were carried out by using epoxides (20 mmol), SNNU-5-M (M = Al, Ga, In) (0.058 mmol), TBAB (0.3 mmol) at 80 °C and 8 bar for 5 h;

b SNNU-5-Al (0.058 mmol), TBAB (0.15 mmol) at 25 °C, 8 bar for 7 h;

c SNNU-5-Al (0.058 mmol), TBAB (0.15 mmol);

d Yields were determined by GC analysis;

e Turnover number (product (mmol)/metal (mmol));

f Turnover frequency (product (mmol)/metal (mmol)/time (h)).

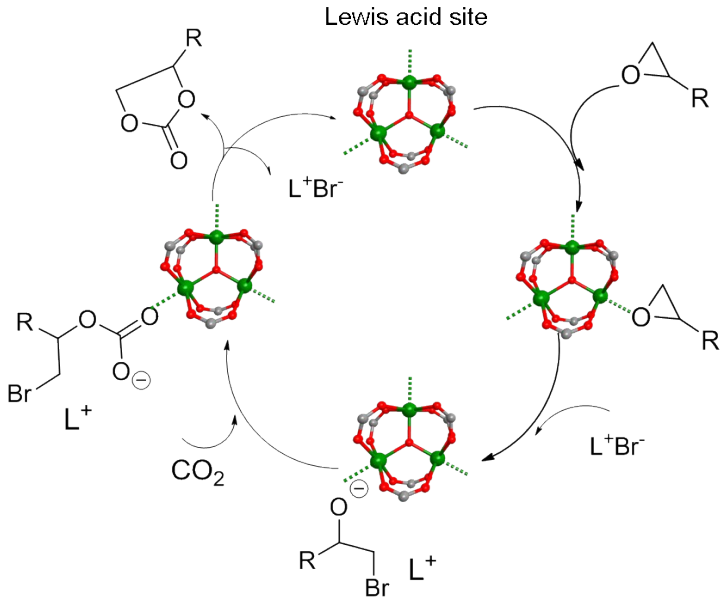

Scheme S1. Proposed catalytic mechanism for the cycloaddition of epoxides and CO_2 over SNNU-5 MOFs.

References

[S1] J. L. C. Rowsell and O. M. Yaghi, *J. Am. Chem. Soc.*, 2006, **128**, 1304-1315.

[S2] A. L. Myers and J. M. Prausnitz, *AIChE J.* 1965, **11**, 121-127.

[S3] Y.-S. Bae, K. L. Mulfort, H. Frost, P. Ryan, S. Punnathanam, L. J. Broadbelt, J. T. Hupp and R. Q. Snurr, *Langmuir*, 2008, **24**, 8592-8598.

[S4] F. Gándara, H. Furukawa, S. Lee and O. M. Yaghi, *J. Am. Chem. Soc.*, 2014, **136**, 5271-5274.

[S5] D. Alezi, Y. Belmabkhout, M. Suyetin, P. M. Bhatt, Ł. J. Weseliński, V. Solovyeva, K. Adil, I. Spanopoulos, P. N. Trikalitis, A.-H. Emwas and M. Eddaoudi, *J. Am. Chem. Soc.*, 2015, **137**, 13308-13318.

[S6] P. Rallapalli, D. Patil, K. P. Prasanth, R. S. Somani, R. V. Jasra and H. C. Bajaj, *J. Porous Mater.*, 2010, **17**, 523-528.

[S7] I. Senkovska, F. Hoffmann, M. Fröba, J. Getzschmann, W. Böhlmann and S. Kaskel, *Microporous Mesoporous Mater.*, 2009, **122**, 93-98.

[S8] P. L. Llewellyn, S. Bourrelly, C. Serre, A. Vimont, M. Daturi, L. Hamon, G. D. Weireld, J. S. Chang, D. Y. Hong, Y. K. Hwang, S. H. Jhung and G. Férey, *Langmuir*, 2008, **24**, 7245-7250.

[S9] S. Bourrelly, P. L. Llewellyn, C. Serre, F. Millange, T. Loiseau and G. Férey, *J. Am. Chem. Soc.*, 2005, **127**, 13519-13521.

[S10] D. Feng, K. Wang, Z. Wei, Y.-P. Chen, C. M. Simon, R. K. Arvapally, R. L. Martin, M. Bosch, T.-F. Liu, S. Fordham, D. Yuan, M. A. Omary, M. Haranczyk, B. Smit and H.-C Zhou, *Nat. Commun.*, 2014, **5**, 5723

[S11] D. Wiersum, J.-S. Chang, C. Serre and P. L. Llewellyn, *Langmuir*, 2013, **29**, 3301-3309.

[S12] O. V. Gutov, W. Bury, D. A. Gomez-Gualdron, V. Krungleviciute, D. Fairen-Jimenez, J. E. Mondloch, A. A. Sarjeant, S. S. Al-Juaid, R. Q. Snurr, J. T. Hupp, T. Yildirim and O. K. Farha, *Chem. Eur. J.*, 2014, **20**, 12389-12393.

[S13] V. Bon, V. Senkovskyy, I. Senkovska and S. Kaskel, *Chem. Commun.*, 2012, **48**, 8407-8409.